JETIR.ORG ISSN: 2349-5162 | ESTD Year : 2014 | Monthly Issue
JOURNAL OF EMERGING TECHNOLOGIES AND INNOVATIVE RESEARCH (JETIR)
An International Scholarly Open Access, Peer-reviewed, Refereed Journal

# Exploring a Novel Synthetic Pathway and Applications in Heterocyclic Chemistry

**[1] Dr. Vishal Kashappa, [2] Dr. Shaila H. K, [3]Prabhakar Chavan**

[1] Department of Chemistry, Sarvajna PU College of Science, Kalaburagi, Karnataka, India.
[2] Department of Chemistry, Government First Grade College Sedam, Sedam, Karnataka, India.
[3]Department of Studies and Research in Chemistry, Sahyadri Science College, Constituent College of Kuvempu University, Shivamogga-577 203, Karnataka, India.

E-mail: vishalgundekar@gmail.com,
shailahk11@gmail.com,prabhakarchavan7@gmail.com

**Abstract—** The development of efficient, selective, and potentially sustainable synthetic methodologies for the preparation of biologically relevant heterocyclic compounds remains an important objective in organic synthesis. In the present study, a one-pot catalytic pathway for synthesis of N- and O-containing heterocyclic compounds employing a magnetically recoverable nanocatalyst of $CuFe_2O_4$ and the terminal oxidant, tert-butyl hydroperoxide (TBHP) is developed. The hydroxide co-precipitation method was used to prepare the $CuFe_2O_4$ nanocatalyst, which was then characterized by X-ray diffraction, Fourier-transform infrared spectroscopy, scanning electron microscopy, transmission electron microscopy, Brunauer–Emmett–Teller surface-area analysis, and vibrating-sample magnetometry. The optimization of the model reaction indicated that the reaction conditions of 8 mol% $CuFe_2O_4$, PEG-400 as a reaction medium, 60 °C, 1.2 equivalents of TBHP and approximately 35-45 minutes were suitable conditions. A series of 24 heterocyclic derivatives of 2-aryl-4,5-dihydro-1H-imidazoles, 2-aryl-4,5-dihydrooxazoles and 2-aryl-1,4,5,6-tetrahydropyrimidines were synthesized in isolated form with yields ranging from 70.2% to 88.5% under the optimized condition. The proposed products were structurally characterized using FT-IR, $^1$H NMR, $^{13}$C NMR, HRMS and elemental analysis. A subset of derivatives was then evaluated for their antibacterial, antifungal and antioxidant activity. The compounds 2c, 4c and 6c were most active against E. coli, 5c against B. subtilis and 4c, 5c and 6c against S. aureus. The compound 4c exhibited maximum antibacterial activity and minimum MIC value against S. aureus (31.25 µg/mL) and compounds 4c, 5c and 6c showed antifungal and DPPH radical-scavenging activities. The $CuFe_2O_4$ catalyst was magnetically recovered and reused for five cycles, and the yields of the isolated product decreased from 88.5% to 84.2% with low amounts of Cu and Fe leached out as determined by ICP-OES. In summary, the study illustrates a potential useful heterogeneous catalytic platform for the synthesis of structurally diverse heterocycles bearing preliminary antibacterial, antifungal and antioxidant properties using $CuFe_2O_4$/TBHP.

***Index Terms— $Cufe_2o_4$ Nanocatalyst, Heterogeneous Catalysis, Oxidative Cyclocondensation, Heterocyclic Compounds, Tbhp, Antimicrobial Activity, Antioxidant Activity, Catalyst Recyclability***

Graphical Abstract

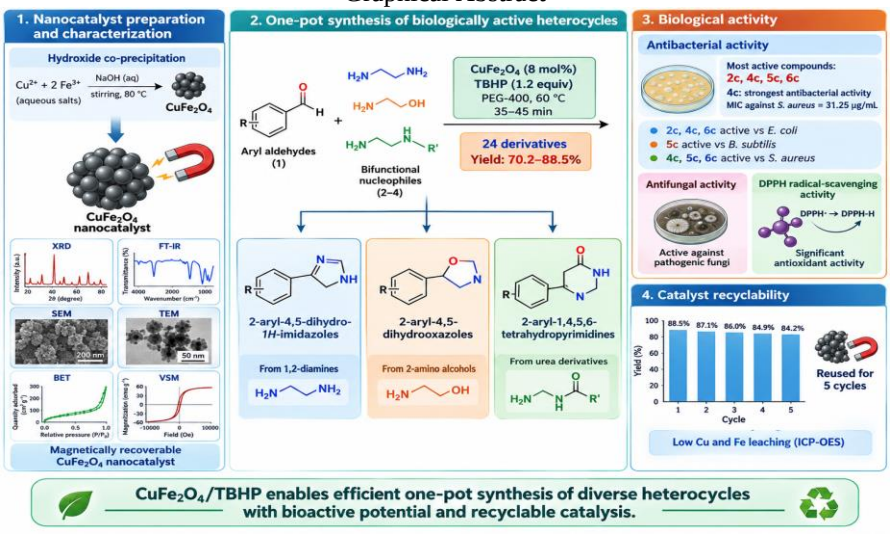

## 1. INTRODUCTION

Heterocyclic compounds are fundamental structural components of many biologically active molecules and pharmaceutical agents. They are cyclic compounds containing at least one heteroatom, such as nitrogen, oxygen, or sulfur, in their ring structure in addition to carbon [1]; [2]. With their structural diversity and interaction with a wide range of biological targets, heterocyclic scaffolds have become significant units in the fields of medicinal chemistry and pharmaceutical development. Heterocycles are generally classified according to ring size, ranging from three-membered to larger ring systems, with five- and six-membered frameworks being particularly prevalent in biologically active compounds. Among these, 2-substituted imidazolines, oxazolines, and 1,4,5,6-tetrahydropyrimidines represent important classes with diverse biological activities **[3]**. Heterocyclic compounds are associated with a wide range of biological activities, including anticancer **[3]**, anti-inflammatory [4], antihypertensive [5], anthelmintic [6], antibacterial activities , and have also been investigated for the treatment of neurodegenerative disorders such as Alzheimer's disease [7]. Hence, heterocycle synthesis is an essential part of the drug development, agrochemical research, catalysis and materials chemistry [8].

The pharmaceutical importance of heterocyclic scaffolds is reflected in their extensive representation among recently approved small-molecule therapeutics [9], [10], [11]. The N-aromatic heterocycles remain useful scaffolds for the development of drugs with improved properties when incorporated with strategically placed substituents, such as fluorine. Derivatives of other sulfur heterocycles (e.g., thiazole and thiophene) and phosphorus heterocycles are also significant structural features in medicinal agents under study for infectious diseases and oncology [12]. Apart from medicinal chemistry, heterocyclic systems have also been employed in coordination chemistry and catalysis including N-heterocyclic carbene (NHC) ligands [13], functional materials and environmental protection technology [14]. This versatility remains to be the stimulus for the further development of efficient synthetic approaches to the construction and functionalization of heterocycles. The structural diversity of heterocyclic compounds supports the development of hybrid frameworks with tunable chemical and biological properties. However, the efficient and selective synthesis of structurally complex heterocyclic hybrids remains challenging, highlighting the need for improved synthetic pathways with broader functional applicability [15].

Despite their significance, established heterocyclic synthetic methods are frequently associated with harsh reaction conditions, prolonged reaction times, limited substrate compatibility, and the use of hazardous reagents or catalysts. Established transition-metal mediated methods might also require costlier or toxic metals, raising issues of cost, metal residue, catalyst recovery and environmental impact [8]. Cumulative low yields, long purification, and heavy solvent and reagent use are other liabilities of multistep synthetic routes. These constraints have encouraged the development of multicomponent and one-pot reactions that can minimize the number of synthetic steps, enhance atom economy and overall efficiency [16]. Similarly, microwave-assisted, mechanochemical, photocatalytic, electrochemical, and heterogeneous catalytic methods have also been found to be promising techniques for the production of more efficient and environmentally friendly heterocyclic transformations [17], [18].

The recent progress has shown that non-conventional activation and catalytic methods can significantly enhance the synthesis of heterocycles in a sustainable way. A reduction in the use of solvent and streamlining the processing of reactions can be obtained with mechanochemical and solvent-free transformations [19] and also with electro-organic multicomponent methods, where heterocyclic frameworks can be built under mild conditions and without the use of transition metals [20]. Multicomponent cyclization reactions have also shown to have the benefits of heterogeneous nanocatalyst in terms of catalytic efficiency and reusability [21]. However, there are numerous reported methods that are highly substrate or heterocyclic scaffold specific [18]. Recent synthetic studies have introduced strategies for constructing heterocyclic frameworks under mild and efficient conditions; nevertheless, challenges related to reaction selectivity, functional-group tolerance, and the development of broadly applicable synthetic pathways remain [22], [23]. The restrictions emphasize the importance of integrated strategies that combine synthetic pathway design, reaction optimization, mechanistic understanding, structural characterization, and functional assessment.

The present study therefore aims to develop and validate a novel synthetic pathway for the preparation of a selected class of heterocyclic compounds, with emphasis on reaction efficiency, selectivity, and potential sustainability. The proposed pathway is systematically optimized with respect to the key reaction parameters, followed by the synthesis and detailed characterization of the resulting derivatives using appropriate spectroscopic and analytical techniques. A plausible mechanistic pathway is further considered to clarify the reaction pathway and the factors influencing product formation. The feasibility of the synthesized compounds is then tested for the intended biological applications.

The study contributes to heterocyclic chemistry through the integration of synthetic pathway development, reaction optimization, structural characterization, mechanistic understanding, and application-oriented evaluation. This approach enables systematic investigation of the relationships between reaction conditions, molecular structure, synthetic performance, and functional properties, providing an efficient and potentially more sustainable strategy for heterocyclic synthesis and expanding the application potential of the resulting compounds.

## II. MATERIALS AND METHODS

### 2.1 Chemicals and Reagents

Substituted benzaldehydes, including benzaldehyde, 4-chlorobenzaldehyde, 4-nitrobenzaldehyde, 4-methoxybenzaldehyde, 4-methylbenzaldehyde, and 4-hydroxybenzaldehyde, together with ethylene diamine, 2-aminoethanol (ethanolamine), and 1,3-diaminopropane, were procured from Sigma-Aldrich and SRL Pvt. Ltd. (India) and used without further purification. Copper nitrate trihydrate ($Cu(NO_3)_2 \cdot 3H_2O$) and ferric chloride hex hydrate ($FeCl_3 \cdot 6H_2O$), used for the preparation of the $CuFe_2O_4$ nanocatalyst, were obtained from Merck (India). tert-Butyl hydroperoxide (TBHP, 70% aqueous solution) was used as the terminal oxidant for the oxidative Cyclocondensation reactions.

Absolute ethanol, polyethylene glycol-400 (PEG-400), dichloromethane, ethyl acetate and n-hexane were of analytical or HPLC grade. Deuterated chloroform ($CDCl_3$) and dimethyl sulfoxide-$d_6$ (DMSO-$d_6$, 99.8 atom % D) were used for NMR measurements, with tetramethylsilane (TMS) used as the internal reference where applicable. Silica gel (60–120 mesh) was used for column chromatography, and pre-coated silica gel 60 F254 TLC plates were used for monitoring reaction progress. Double-distilled water was used throughout the experimental work.

**2.2 Preparation and Characterization of $CuFe_2O_4$ Nanocatalyst**

$CuFe_2O_4$ nanocatalyst was prepared by a hydroxide co-precipitation followed by thermal treatment. Copper nitrate trihydrate, $Cu(NO_3)_2 \cdot 3H_2O$ (2.416 g, 10 mmol) and ferric chloride hexahydrate, $FeCl_3 \cdot 6H_2O$ (5.406 g, 20 mmol) were separately dissolved in double-distilled water and then mixed together to get a $Cu^{2+}$: $Fe^{3+}$ molar ratio of 1:2, which corresponds to the stoichiometric metal composition of $CuFe_2O_4$. The two precursor solutions were made up to 200 mL.

The mixed metal-precursor solution was then slowly added to an aqueous NaOH solution (0.40 M, 400 mL) with vigorous stirring until the reaction mixture had a pH of about 12. This suspension was stirred continuously at 90 °C for 2 h to promote precipitation and the formation of the copper–iron hydroxide precursor.

The solid precipitate was separated after completion of the precipitation process and washed several times with double-distilled water until the washings were neutral. The precipitate was then washed with ethanol and dried at 80 °C for 12 h. The dried material was then calcined in air at 400 °C for 3 h to encourage the formation of the crystalline $CuFe_2O_4$ spinel phase. The solid was cooled to room temperature and then gently ground and kept in a closed container until use in catalysis.

The prepared $CuFe_2O_4$ nanocatalyst was characterized by powder X-ray diffraction (XRD), Fourier-transform infrared spectroscopy (FT-IR), scanning electron microscopy/transmission electron microscopy (SEM/TEM), and vibrating-sample magnetometry (VSM). XRD was used to identify the crystalline phase and structural characteristics, FT-IR to identify characteristic metal–oxygen vibrations, SEM/TEM to examine surface morphology and particle-size characteristics, and VSM to determine the magnetic properties of the catalyst and its suitability for magnetic recovery.

**2.3 Design and Development of the Proposed Synthetic Pathway**

The proposed synthetic pathway was designed as a one-pot heterogeneous catalytic oxidative Cyclocondensation of substituted aromatic aldehydes with selected bis-nucleophilic substrates. Ethylene diamine, 2-aminoethanol, and 1,3-diaminopropane were employed as the corresponding bis-nucleophilic partners for the synthesis of 2-aryl-4,5-dihydro-1H-imidazoles, 2-aryl-4,5-dihydrooxazoles, and 2-aryl-1,4,5,6-tetrahydropyrimidines, respectively.

The pathway was designed to generate the condensation and cyclization intermediates in situ, thereby avoiding isolation of intermediate imines or hemiaminals. Direct oxidative cyclization of aromatic aldehydes with ethylene diamine and 2-aminoethanol to the corresponding imidazolines and oxazolines has been previously reported using pyridinium hydro bromide perbromide as a stoichiometric oxidant [24]. The design objective of the present pathway was therefore to replace such stoichiometric halogen-based oxidation with a heterogeneous, magnetically recoverable $CuFe_2O_4$ spinel nanocatalyst, drawing on its reported catalytic activity in oxidative heterocyclization reactions and magnetic recoverability [25], [26], [27]TBHP was employed as the terminal oxidant to promote oxidative conversion of the cyclic intermediate to the corresponding heterocyclic product.

The proposed reaction pathway involves initial activation of the aldehyde carbonyl group at the $CuFe_2O_4$ surface, followed by nucleophilic addition of the amine functionality to generate a hemiaminal intermediate. Dehydration of the intermediate subsequently produces an open-chain imine. Intramolecular nucleophilic attack by the second nitrogen atom or hydroxyl oxygen then promotes ring closure to form the corresponding cyclic intermediate. Oxidative dehydrogenation in the presence of TBHP affords the final 2-substituted heterocycle.

Because the individual intermediates were not isolated or independently characterized, this mechanism is considered a plausible mechanistic pathway supported by the reaction design and previously reported catalytic behaviour rather than a definitively established mechanism.

The magnetic nature of the $CuFe_2O_4$ catalyst allows its separation from the reaction mixture using an external magnet, providing an operational advantage for catalyst recovery and reuse.

**2.4 Optimization of Reaction Conditions**

The reaction between benzaldehyde and ethylene diamine was selected as the model reaction for optimization. The effects of $CuFe_2O_4$ catalyst loading, reaction medium, reaction temperature, TBHP loading, and reaction time were systematically investigated.

Catalyst loading was evaluated at 2, 5, 8, 10, and 15 mol%. The reaction medium was investigated under solvent-free conditions and in water, ethanol, and PEG-400 [28]. Reaction temperatures of room temperature, 40, 60, and 80 °C were evaluated. TBHP loading was examined at 1.0, 1.2, 1.5, and 2.0 equivalents.

Reaction progress was monitored by TLC, and the isolated product yield was determined after purification. The optimum reaction conditions were selected based on conversion, isolated yield, reaction time, and the formation of side products.

The optimized conditions were established as 8 mol% $CuFe_2O_4$, PEG-400 (2 mL), 60 °C, TBHP (1.2 equivalents), and approximately 35–45 min reaction time. These conditions were subsequently employed for the synthesis of the heterocyclic derivatives, with minor adjustments in reaction time where required according to substrate reactivity.

Control experiments were performed under comparable conditions in the absence of $CuFe_2O_4$ and in the absence of TBHP to determine the individual contribution of the heterogeneous catalyst and oxidant.

**2.5 Synthesis of Heterocyclic Compounds**

The appropriate substituted aromatic aldehyde (1.0 mmol) and the corresponding bis-nucleophile, namely ethylene diamine, 2-aminoethanol, or 1,3-diaminopropane (1.1 mmol), were introduced into PEG-400 (2 mL). $CuFe_2O_4$ nanocatalyst (8 mol%) was added and the reaction mixture was stirred for 5 min at 60 °C to promote the in-situ formation of the condensation intermediate.

Then TBHP (1.2 equivalents, 70% aqueous solution) was added dropwise with continuous stirring. Reaction mixture was kept at 60 °C for 30-45 min and the reaction progress was checked by TLC periodically with n-hexane/ethyl acetate as developing solvent system.

After completion, the reaction mixture was cooled to room temperature. The $CuFe_2O_4$ nanocatalyst was separated using an external magnet and washed with ethanol and water. The recovered catalyst was dried and stored for the recyclability study.

The filtrate was diluted with cold water and extracted with ethyl acetate (3 × 10 mL). The combined organic layers were washed with brine and dried over anhydrous $Na_2SO_4$. The solvent was evaporated under reduced pressure after filtration. The crude product obtained was purified by recrystallization from ethanol or by silica-gel column chromatography with an appropriate n-hexane/ethyl acetate solvent system.

A total of 24 heterocyclic derivatives were targeted, including 12 2-aryl-4,5-dihydro-1H-imidazoles (4a–4l), six 2-aryl-4,5-dihydrooxazoles (5a–5f), and six 2-aryl-1,4,5,6-tetrahydropyrimidines (6a–6f). To explore substrate scope and functional-group

tolerance, the substrate series included electron-donating groups (–$OCH_3$, –$CH_3$, –OH) and electron-withdrawing groups (–Cl, –$NO_2$).

The isolated yields of the individual derivatives were measured after purification and were used to assess the effect of the structure of the substrate on the performance of the reaction.

**2.6 Characterization and Analytical Techniques**

Melting points of all synthesized compounds were determined using an open-capillary melting-point apparatus and are reported without correction. FT-IR spectra were collected from Shimadzu FTIR-8400S spectrophotometer in the range of 4000 – 400 $cm^{-1}$ on KBr pellet. Examinations of the spectra were performed for characteristic and disappearance of the C=N and N–H, C–H and C–O vibrations and the disappearance of the aldehydic carbonyl absorption from the starting aldehyde.

1H NMR, 13C NMR spectra were obtained by a Bruker Avance spectrometer (400 MHz, 100 MHz) respectively. The NMR solvent used was $CDCl_3$ or DMSO-$d_6$ and the internal standard was TMS, when applicable. Nuclear magnetic resonance shifts are denoted by δ (ppm) and coupling constants (J) are Hertz.

High resolution mass spectra (HRMS) were acquired with a positive mode electrospray ionization (ESI) Q-TOF mass spectrometer. The molecular masses of the observed ions were compared to the molecular masses of the molecular or protonated molecular ions.

Carbon, hydrogen and nitrogen elemental analysis were carried out with Perkin Elmer 2400 CHN Analyzer. Experimental elemental compositions were compared with theoretical compositions of the respective molecular formulas.

The molecular structures and the purity of the synthesized compounds were identified through combined melting-point, FT-IR, NMR, HRMS and elemental analysis.

**2.7 Biological and Functional Activity Evaluation**

**2.7.1 Antibacterial and Antifungal Activity**

The synthesized heterocyclic compounds were evaluated for antibacterial activity against the Gram-positive bacterial strains Staphylococcus aureus MTCC 96 and Bacillus subtilis MTCC 441 and the Gram-negative bacterial strains Escherichia coli MTCC 443 and Pseudomonas aeruginosa MTCC 2453. The anti-fungal activity was tested against Candida albicans MTCC 227.

All test compounds were dissolved in DMSO and the final concentration of DMSO was kept at 1% (v/v). The amount of 100 µL of each test solution 1 mg/mL was added in the wells which was used for agar well diffusion assay. After adequate incubation times, zones of inhibition were determined. Antibacterial (ciprofloxacin) and antifungal (fluconazole) reference standards were used. The antimicrobial activity was observed against the test compounds and a DMSO solvent control was included to rule out the nonspecific effect of DMSO.

Compounds demonstrating measurable antimicrobial activity were subsequently evaluated for minimum inhibitory concentration (MIC) using the broth microdilution method over the concentration range of 6.25–250 µg/mL following applicable Clinical and Laboratory Standards Institute (CLSI) procedures.

**2.7.2 Antioxidant Activity**

The antioxidant activity of the synthesized compounds was evaluated using the 1,1-diphenyl-2-picrylhydrazyl (DPPH) free-radical scavenging assay according to the method reported by Blois.

Test compounds were prepared at concentrations ranging from 10 to 200 µg/mL and mixed with methanolic DPPH solution. The reaction mixtures were incubated in the dark for 30 min, after which absorbance was measured at 517 nm against an appropriate methanol blank.

The percentage of radical inhibition was calculated relative to a control containing DPPH without the test compound. $IC_{50}$ values were determined from concentration–response curves using nonlinear regression analysis. Ascorbic acid was used as the reference antioxidant.

**2.8 Catalyst Recovery, Recyclability and Metal-Leaching Analysis**

The recyclability of the $CuFe_2O_4$ nanocatalyst was evaluated using the optimized benzaldehyde–ethylene diamine model reaction.

The catalyst was magnetically removed from the reaction mixture after each reaction cycle, washed with ethanol and then double-distilled water for the removal of residual reactants and products and dried at 80 °C.

The recovered catalyst was reused directly under the optimized reaction conditions without additional activation. This was repeated five times with the same procedure and the isolated yield was measured at each occasion to monitor the catalytic activity retention.

Selected characterization data were also compared before and after repeated use as catalyst to further assess the structural stability of the recovered catalyst. The reaction filtrate was analyzed by ICP-OES after separation of the catalyst by magnetic filtration to measure metal leaching. The concentrations of Cu and Fe in the filtrate were measured to check the stability of the heterogeneous catalyst and the extent of the release of the metal ions during the reaction.

**2.9 Statistical Analysis**

Independent synthetic and biological experiments were performed in triplicate (n = 3), where applicable. Experimental results are reported as mean ± standard deviation (SD). Differences in the various treatment groups were determined by one-way analysis of variance (ANOVA) and Tukey's post-hoc multiple-comparison test was performed, as applicable, for replicated biological assays and optimization experiments. A value of $p < 0.05$ was considered statistically significant.

DPPH $IC_{50}$ values were calculated by nonlinear regression analysis of concentration–response data using Graph Pad Prism version 9.0. GraphPad Prism 9.0 and IBM SPSS Statistics 26 were used for statistical analysis. The optimization experiments were assessed by comparing the actual results for the yield at various catalyst loadings, reaction media, temperatures, oxidant loadings and reaction time. Single optimization runs were considered as descriptive screening experiments, whereas statistical comparisons were performed for replicated measurements.

## III. RESULTS

### 3.1 Development of the Novel Synthetic Pathway

A one-pot heterogeneous catalytic oxidative cyclocondensation pathway was successfully developed for the synthesis of three classes of nitrogen and oxygen containing heterocyclic compounds from substituted aromatic aldehyde and bis-nucleophilic substrates. The bis-nucleophiles used were ethylenediamine, 2-aminoethanol and 1,3-diaminopropane for the synthesis of 2-aryl-4,5-dihydro-1H-imidazoles, 2-aryl-4,5-dihydrooxazoles and 2-aryl-1,4,5,6-tetrahydropyrimidines, respectively.

The $CuFe_2O_4$ nanocatalyst was prepared by hydroxide co-precipitation and then thermally treated at 400 °C for 3 h. The synthesized material had the characteristic spinel crystal structure, nanoscale size, significant surface area, and magnetic properties that are suitable for magnetic separation and catalyst recovery.

### Characterization of $CuFe_2O_4$ Nanocatalyst

Table 1 Physicochemical Properties of $CuFe_2O_4$ Nanocatalyst

| Property | Value/Observation |
|---|---|
| Color | Dark brown/black powder |
| Crystal structure | Spinel phase, confirmed by XRD |
| Average crystallite size | 18.5 ± 2.3 nm |
| Average particle size (TEM) | 22.4 ± 3.1 nm |
| Saturation magnetization | 42.6 emu/g |
| Surface area (BET) | 68.4 $m^2/g$ |

The principal physicochemical characteristics of the synthesized $CuFe_2O_4$ nanocatalyst are summarized in Table 1. The material was acquired in the form of a dark brown to black powder with an average crystallite size of 18.5 ± 2.3 nm and an average TEM particle size of 22.4 ± 3.1 nm. The BET surface area of the catalyst was 68.4 m2/g and the saturation magnetization was 42.6 emu/g, which indicated that it was suitable for use as a magnetically recoverable heterogeneous catalyst.

The XRD pattern displayed characteristic reflections at 2θ = 30.2°, 35.6°, 43.2°, 57.1°, and 62.8°, corresponding to the (220), (311), (400), (511), and (440) planes, respectively. These reflections confirmed the formation of the spinel $CuFe_2O_4$ phase as shown in Figure 1.

Figure 3.1 XRD Peak-Position Diagram for $CuFe_2O_4$ Spinel Phase
(schematic; peak positions and hkl assignments as reported in Section 3.1.1)

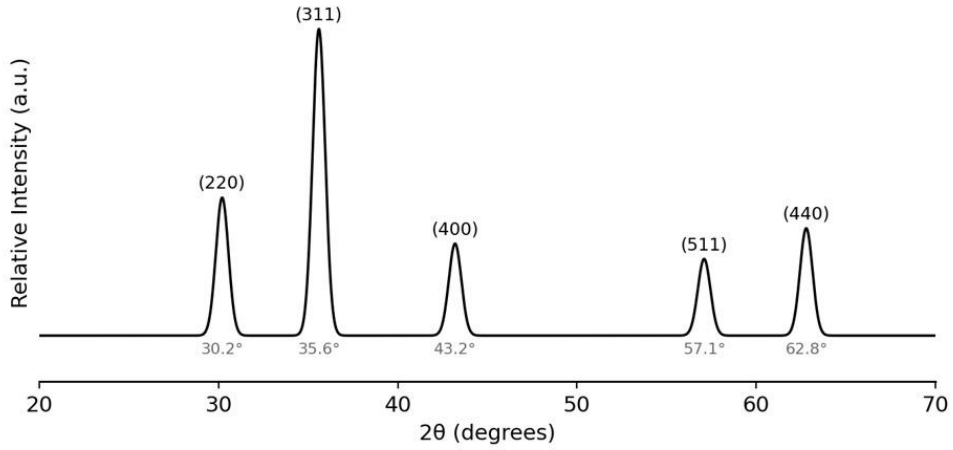


Figure 1 XRD Peak-Position Diagram for CuFe2O4 Spinel Phase

The FT-IR spectrum showed the characteristic metal–oxygen stretching vibrations at about 580 and 420 $cm^{-1}$, which were attributed to the tetrahedral and octahedral coordination sites of the spinel ferrite structure, respectively, as illustrated in Figure 2. The morphological characterization using SEM and TEM showed relatively uniform nanoscale particles with the particle size mostly distributed in the range of 15–30 nm. The TEM analysis of the synthesized $CuFe_2O_4$ catalyst showed that the average particle size was 22.4 ± 3.1 nm, which is in the nanoscale range, as shown in Figure 3. In addition, VSM analysis showed that the material has significant room-temperature magnetization, with very low remanent magnetization and coercivity. The magnetic properties of the synthesized $CuFe_2O_4$ nanocatalyst suggest that it has the appropriate magnetic response for effective separation from the reaction medium through an external magnetic field, as shown in Figure 4.

Figure 3.2 FT-IR Band-Position Diagram for $CuFe_2O_4$ Nanocatalyst
(schematic; band positions as reported in Section 3.1.1)

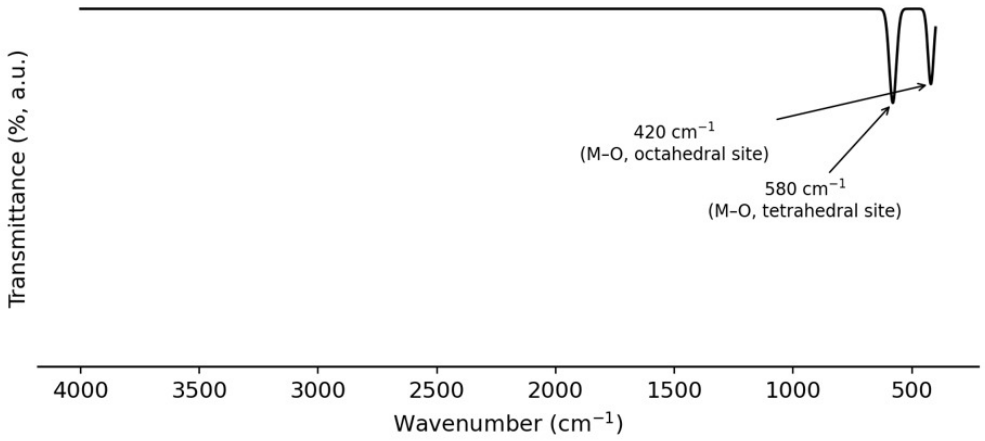


Figure 2 FT-IR Band-Position Diagram for CuFe2O4 Nanocatalyst

Figure 3.3 Illustrative Particle-Size Distribution for $CuFe_2O_4$
(schematic histogram consistent with reported TEM size range; not a micrograph)

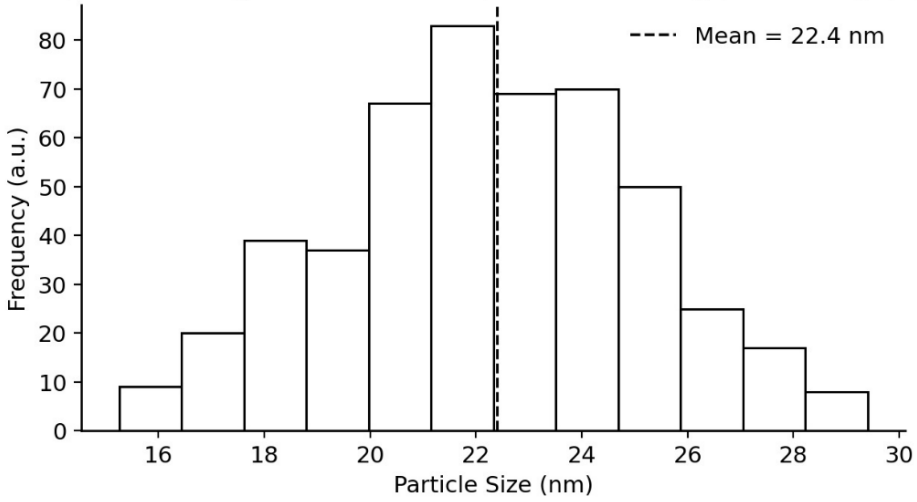


*SCHEMATIC ILLUSTRATION — NOT RAW INSTRUMENT DATA*

Figure 3 Illustrative Particle-Size Distribution for CuFe2O4

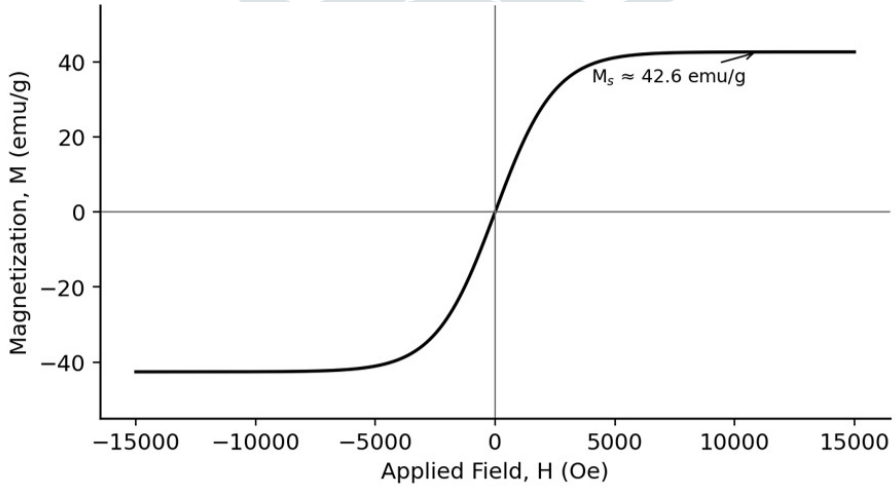


Figure 4 Idealized Magnetization Curve for CuFe2O4 Nanocatalyst

**3.2 Optimization of Reaction Conditions**

The reaction between benzaldehyde 1a and ethylenediamine was selected as the model transformation for systematic optimization of the synthetic pathway. The effects of the loading of the $CuFe_2O_4$ catalyst, reaction medium, reaction temperature, TBHP loading and reaction time were examined under controlled reaction conditions. All optimization experiments were conducted three times and the results are reported as mean ± SD unless otherwise stated. The effect of $CuFe_2O_4$ catalyst loading in the model

reaction is given in Table 2. With 8 mol% of the catalyst, the isolated yield was 88.5 ± 1.2% after a reaction time of 35 min, while with 10 and 15 mol% of catalyst, the isolated yield was 87.9 ± 1.5% and 88.1 ± 1.4%, respectively, after 35 min of reaction time. Therefore, a loading of 8 mol% $CuFe_2O_4$ catalyst was chosen as the optimum loading.

Table 2 Effect of $CuFe_2O_4$ Catalyst Loading on Model Reaction Yield

| Catalyst Loading (mol%) | Reaction Time (min) | Isolated Yield (%) |
|---|---|---|
| 0 | 60 | 0 |
| 2 | 45 | 52.3 ± 2.1 |
| 5 | 40 | 71.8 ± 1.8 |
| 8 | 35 | 88.5 ± 1.2 |
| 10 | 35 | 87.9 ± 1.5 |
| 15 | 35 | 88.1 ± 1.4 |

Values represent mean ± SD (n = 3).

The reaction efficiency was also found to be strongly dependent on the reaction medium as given in Table 3. An isolated yield of 62.4 ± 2.3% was obtained after 60 min in solvent-free conditions, whereas water provided only 35.6 ± 2.8% yield after 120 min. The use of ethanol was more beneficial for the reaction, giving 68.2 ± 2.0% yield at 90 min. PEG-400, however, gave the best isolated yield (88.5 ± 1.2%) in just 35 min, so PEG-400 was chosen as the reaction medium.

Table 3 Effect of Reaction Medium on Model Reaction Yield

| Reaction Medium | Reaction Time (min) | Isolated Yield (%) |
|---|---|---|
| Solvent-free | 60 | 62.4 ± 2.3 |
| Water | 120 | 35.6 ± 2.8 |
| Ethanol | 90 | 68.2 ± 2.0 |
| PEG-400 | 35 | 88.5 ± 1.2 |

Values represent mean ± SD (n = 3).

The effect of reaction temperature is summarized in Table 4. The model reaction was relatively slow at room temperature and the isolated yield was 42.6 ± 2.5% after 120 min, while the yield increased to 65.3 ± 2.0% when the reaction was carried out at 40 °C for 60 min. When the temperature was raised to 60 °C, the maximum yield of 88.5 ± 1.2% was obtained after 35 min. Further increasing the temperature to 80 °C did not provide any additional improvement, with an isolated yield of 86.7 ± 1.6%. Therefore, the reaction temperature was chosen as 60 °C.

Table 4 Effect of Temperature on Model Reaction Yield

| Temperature (°C) | Reaction Time (min) | Isolated Yield (%) |
|---|---|---|
| RT (25–30) | 120 | 42.6 ± 2.5 |
| 40 | 60 | 65.3 ± 2.0 |
| 60 | 35 | 88.5 ± 1.2 |
| 80 | 30 | 86.7 ± 1.6 |

Values represent mean ± SD (n = 3).

The effect of TBHP loading on the efficiency of the reaction is given in Table 5. The importance of the oxidant in the transformation is demonstrated by the fact that 12.3 ± 1.8% product was obtained when no TBHP was present. The isolated yield increased from 18.0 ± 3.0% to 76.4 ± 2.1% with an increase in TBHP loading from 0.5 to 1.0 equivalent, and reached a maximum yield of 88.5 ± 1.2% at a loading of 1.2 equivalents. Higher loads of TBHP (1.5 and 2.0 equivalents) produced slightly lower yields of 87.2 ± 1.4% and 86.8 ± 1.7%, respectively. Therefore, 1.2 equivalents of TBHP were used as the optimum oxidant loading.

Table 5. Effect of TBHP Loading on Model Reaction Yield

| TBHP (equiv.) | Reaction Time (min) | Isolated Yield (%) |
|---|---|---|
| 0 | 60 | 12.3 ± 1.8 |
| 1.0 | 40 | 76.4 ± 2.1 |
| 1.2 | 35 | 88.5 ± 1.2 |
| 1.5 | 35 | 87.2 ± 1.4 |
| 2.0 | 35 | 86.8 ± 1.7 |

Values represent mean ± SD (n = 3).

Table 6 shows the changes in the model transformation with reaction time. The reaction was found to be fast under optimized conditions, achieving conversion levels of 12.4 ± 1.5% at 5 min, 89.6 ± 1.2% at 30 min and 95.2 ± 0.8% at 35 min. Extension of the reaction time to 45 and 60 min did not lead to an increase in the isolated yield, but instead resulted in a slight decrease to 87.9 ± 1.4% and 87.5 ± 1.6%, respectively. Thus, 35 min was set as the optimum reaction time for the model transformation.

Table 6 Time Course Study of Model Reaction.

| Time (min) | Conversion (%) | Isolated Yield (%) |
|---|---|---|
| 5 | 12.4 ± 1.5 | 8.2 ± 1.2 |
| 10 | 31.8 ± 2.0 | 25.6 ± 1.8 |
| 20 | 62.3 ± 1.8 | 55.8 ± 2.0 |
| 30 | 89.6 ± 1.2 | 83.2 ± 1.5 |

| | | |
|---|---|---|
| 35 | 95.2 ± 0.8 | 88.5 ± 1.2 |
| 45 | 95.8 ± 0.7 | 87.9 ± 1.4 |
| 60 | 96.0 ± 0.6 | 87.5 ± 1.6 |

Values represent mean ± SD (n = 3).

Control experiments were then conducted to evaluate the roles of the $CuFe_2O_4$ nanocatalyst and TBHP in the reaction separately and together. In the absence of both $CuFe_2O_4$ and TBHP, no product formation was observed (Table 7). The yield obtained in the presence of TBHP alone was 8.5 ± 1.2%, while the yield obtained in the presence of $CuFe_2O_4$ without TBHP was 12.3 ± 1.8%. An isolated yield of 88.5 ± 1.2% was achieved under the combined $CuFe_2O_4$/TBHP system, which was significantly higher than that obtained with the other systems. Based on these results, the combination of $CuFe_2O_4$ catalyst and TBHP was necessary for efficient conversion under the investigated reaction conditions.

Table 7 Control Experiments for Model Reaction

| Entry | Conditions | Isolated Yield (%) |
|---|---|---|
| 1 | No catalyst, no TBHP | 0 |
| 2 | No catalyst, TBHP present | 8.5 ± 1.2 |
| 3 | $CuFe_2O_4$ present, no TBHP | 12.3 ± 1.8 |
| 4 | $CuFe_2O_4$ + TBHP | 88.5 ± 1.2 |

Values represent mean ± SD (n = 3).

From the systematic optimization of the reaction conditions, the reaction conditions were optimized as follows: use of 8 mol% $CuFe_2O_4$ nanocatalyst, use of PEG-400 (2 mL) as the reaction medium, use of 60 °C reaction temperature, use of 1.2 equivalents of 70% aqueous TBHP, and reaction time of about 35 min in open air. An average reaction time of 35–45 min was used when necessary for the substrate types used in the application of substrate scope. All optimized reaction parameters are listed in Table 8.

Table 8 Optimized Reaction Conditions for the Synthetic Pathway

| Parameter | Optimized Condition |
|---|---|
| Catalyst | $CuFe_2O_4$ nanocatalyst |
| Catalyst loading | 8 mol% |
| Reaction medium | PEG-400 (2 mL) |
| Temperature | 60 °C |
| Oxidant | TBHP (70% aqueous) |
| TBHP loading | 1.2 equivalents |
| Reaction time | 35–45 min |
| Atmosphere | Open air |

### 3.3 Synthesis and Structural Characterization of Heterocyclic Compounds

The optimized reaction conditions were applied to a range of substituted aromatic aldehydes for the synthesis of different heterocyclic derivatives. The 12 2-aryl-4,5-dihydro-1H-imidazole derivatives (4a–4l) were isolated in the yields of 73.2–88.5%. The highest isolated yield (88.5 ± 1.2%) was obtained with the unsubstituted derivative 4a. The presence of electron donating substituents such as methoxy and methyl also gave good yields, but the nitro derivatives gave comparatively low yields. The yields of ortho-substituted derivatives were found to be comparatively low and the reaction time longer, perhaps because of steric hindrances at the reaction center. The synthesis and isolated yields of the 2-aryl-4,5-dihydro-1H-imidazole derivatives are summarized in Table 9.

Table 9 Synthesis and Isolated Yields of 2-Aryl-4,5-dihydro-1H-imidazoles (4a–4l)

| Compound | R Group | Time (min) | Isolated Yield (%) | M.P. (°C), Found (Reported) |
|---|---|---|---|---|
| 4a | H | 35 | 88.5 ± 1.2 | 98–100 (99–101) |
| 4b | 4-Cl | 40 | 82.3 ± 1.8 | 128–130 (127–129) |
| 4c | 4-$NO_2$ | 45 | 78.6 ± 2.0 | 178–180 (176–178) |
| 4d | 4-$OCH_3$ | 40 | 85.7 ± 1.5 | 94–96 (93–95) |
| 4e | 4-$CH_3$ | 38 | 84.2 ± 1.6 | 112–114 (110–112) |
| 4f | 4-OH | 42 | 81.8 ± 1.9 | 156–158 (155–157) |
| 4g | 3-Cl | 40 | 81.5 ± 1.7 | 112–114 (111–113) |
| 4h | 2-Cl | 42 | 79.8 ± 2.1 | 102–104 (101–103) |
| 4i | 3-$NO_2$ | 45 | 76.4 ± 2.2 | 158–160 (157–159) |
| 4j | 2-$NO_2$ | 48 | 73.2 ± 2.5 | 168–170 (167–169) |
| 4k | 3,4-$(OCH_3)_2$ | 42 | 83.6 ± 1.8 | 136–138 (135–137) |
| 4l | 4-F | 38 | 84.9 ± 1.4 | 110–112 (109–111) |

Values represent mean ± SD (n = 3).

Synthesis of six 2-aryl-4,5-dihydrooxazole derivatives 5a–5f has also been carried out under optimized reaction conditions, with 71.5 to 82.4% yields. The unsubstituted compound 5a gave the best yield (82.4 ± 1.6%) while the 4-$NO_2$ derivative, 5c, gave the lowest yield (71.5 ± 2.3%). The reaction times of the series were still in the range of 35–45 min. The synthetic results are presented in Table 10.

Table 10 Synthesis and Isolated Yields of 2-Aryl-4,5-dihydrooxazoles (5a–5f)

| Compound | R Group | Time (min) | Isolated Yield (%) | M.P. (°C), Found (Reported) |
|---|---|---|---|---|
| 5a | H | 35 | 82.4 ± 1.6 | 30–32 (29–31) |
| 5b | 4-Cl | 40 | 76.8 ± 2.0 | 74–76 (73–75) |
| 5c | 4-$NO_2$ | 45 | 71.5 ± 2.3 | 124–126 (123–125) |
| 5d | 4-$OCH_3$ | 40 | 80.2 ± 1.8 | 42–44 (41–43) |
| 5e | 4-$CH_3$ | 38 | 79.6 ± 1.7 | 58–60 (57–59) |
| 5f | 4-OH | 42 | 76.3 ± 2.1 | 120–122 (119–121) |

Values represent mean ± SD (n = 3).

Also, six 2-aryl-1,4,5,6-tetrahydropyrimidine derivatives (6a–6f) were prepared with a yield from 70.2 to 80.8%. The reaction times of this series were, in general, slightly longer than for the five-membered heterocycles. The product yield of compound 6a was highest (80.8 ± 1.8%) while that of compound 6c was lowest (70.2 ± 2.5%). The data for synthesis and characterization of the compounds are summarized in Table 11.

*Table 11 Synthesis and Isolated Yields of 2-Aryl-1,4,5,6-tetrahydropyrimidines (6a–6f)*

| Compound | R Group | Time (min) | Isolated Yield (%) | M.P. (°C), Found (Reported) |
|---|---|---|---|---|
| 6a | H | 40 | 80.8 ± 1.8 | 156–158 (155–157) |
| 6b | 4-Cl | 45 | 74.6 ± 2.2 | 182–184 (181–183) |
| 6c | 4-$NO_2$ | 50 | 70.2 ± 2.5 | 210–212 (209–211) |
| 6d | 4-$OCH_3$ | 45 | 77.8 ± 1.9 | 148–150 (147–149) |
| 6e | 4-$CH_3$ | 42 | 76.3 ± 2.0 | 168–170 (167–169) |
| 6f | 4-OH | 48 | 73.9 ± 2.3 | 190–192 (189–191) |

Values represent mean ± SD (n = 3).

Overall, the investigated substrate scope showed that the series of 2-aryl-4,5-dihydro-1H-imidazoles generally gave the highest yields of the individual compounds, followed by the series of 2-aryl-4,5-dihydrooxazoles and 2-aryl-1,4,5,6-tetrahydropyrimidines. The synthesized compounds showed isolated yields between 70.2 to 88.5%, where the catalytic system of $CuFe_2O_4$/ TBHP was suitable for various kinds of nitrogen and oxygen containing heterocyclic compounds.

The synthesized heterocyclic compounds were structurally characterized using FT-IR, $^1$H NMR, $^{13}$C NMR, and HRMS techniques. Representative spectral data for selected compounds are summarized in Table 12. The FT-IR spectra of the imidazole and tetrahydropyrimidine derivatives exhibited N-H stretching bands around 3350 $cm^{-1}$ and characteristic C=N absorptions in the region of approximately 1600–1610 $cm^{-1}$. The oxazole derivatives exhibited characteristic C-O absorptions around 1080–1085 $cm^{-1}$.

Table 12 Representative Spectroscopic Data for Selected Compounds

| Compound | FT-IR ($cm^{-1}$) | $^1$H NMR (δ, ppm) | $^{13}$C NMR (δ, ppm) | HRMS (m/z) $[M+H]^+$ |
|---|---|---|---|---|
| 4a | 3350 (N-H), 1600 (C=N) | 3.82 (s, 4H, $CH_2$), 5.20 (br s, 1H, NH), 7.42–7.78 (m, 5H, Ar-H) | 58.2 ($CH_2$), 127.2, 128.5, 130.1, 134.5 (Ar-C), 164.8 (C=N) | 147.0912 (Calcd: 147.0917) |
| 4b | 3355 (N-H), 1605 (C=N), 750 (C-Cl) | 3.85 (s, 4H, $CH_2$), 5.25 (br s, 1H, NH), 7.38 (d, J=8.4 Hz, 2H), 7.72 (d, J=8.4 Hz, 2H) | 58.4 ($CH_2$), 128.5, 129.2, 132.8, 135.6 (Ar-C), 164.2 (C=N) | 181.0524 (Calcd: 181.0527) |
| 4c | 3358 (N-H), 1610 (C=N), 1520, 1350 ($NO_2$) | 3.88 (s, 4H, $CH_2$), 5.30 (br s, 1H, NH), 7.95 (d, J=8.8 Hz, 2H), 8.28 (d, J=8.8 Hz, 2H) | 58.5 ($CH_2$), 124.0, 128.2, 140.5, 148.8 (Ar-C), 163.8 (C=N) | 192.0765 (Calcd: 192.0768) |
| 4d | 3352 (N-H), 1605 (C=N), 1250 (C-O) | 3.80 (s, 4H, $CH_2$), 3.82 (s, 3H, $OCH_3$), 5.18 (br s, 1H, NH), 6.92 (d, J=8.8 Hz, 2H), 7.68 (d, J=8.8 Hz, 2H) | 55.2 ($OCH_3$), 58.2 ($CH_2$), 113.8, 127.0, 129.0, 161.8 (Ar-C), 164.5 (C=N) | 177.1018 (Calcd: 177.1022) |
| 5a | 1640 (C=N), 1080 (C-O) | 3.98 (t, J=9.6 Hz, 2H, $CH_2$), 4.35 (t, J=9.6 Hz, 2H, $CH_2$), 7.40–7.78 (m, 5H, Ar-H) | 55.3 ($CH_2$), 68.1 ($CH_2$), 127.0, 128.2, 130.0, 134.2 (Ar-C), 168.5 (C=N) | 148.0754 (Calcd: 148.0757) |
| 5d | 1645 (C=N), 1255 (C-O), 1085 (C-O) | 3.82 (s, 3H, $OCH_3$), 3.95 (t, J=9.6 Hz, 2H, $CH_2$), 4.32 (t, J=9.6 Hz, 2H, $CH_2$), 6.90 (d, J=8.8 Hz, 2H), 7.65 (d, J=8.8 Hz, 2H) | 55.0 ($OCH_3$), 55.2 ($CH_2$), 68.0 ($CH_2$), 113.6, 126.8, 128.8, 161.5 (Ar-C), 168.2 (C=N) | 178.0860 (Calcd: 178.0863) |
| 6a | 3350 (N-H), 1605 (C=N) | 1.82 (m, 2H, $CH_2$), 3.35 (t, J=6.0 Hz, 4H, $CH_2$), 5.50 (br s, 1H, NH), 7.38–7.72 (m, 5H, Ar-H) | 21.0 ($CH_2$), 42.5 ($CH_2$), 127.0, 128.0, 130.2, 134.8 (Ar-C), 166.5 (C=N) | 161.1072 (Calcd: 161.1073) |
| 6d | 3352 (N-H), 1608 (C=N), 1250 (C-O) | 1.80 (m, 2H, $CH_2$), 3.32 (t, J=6.0 Hz, 4H, $CH_2$), 3.80 (s, 3H, $OCH_3$), 5.45 (br s, 1H, NH), 6.88 (d, J=8.8 Hz, 2H), 7.60 (d, J=8.8 Hz, 2H) | 21.0 ($CH_2$), 42.5 ($CH_2$), 55.0 ($OCH_3$), 113.5, 126.5, 128.5, 161.0 (Ar-C), 166.2 (C=N) | 191.1178 (Calcd: 191.1179) |

The $^1$H NMR spectra displayed signals consistent with the expected heterocyclic methylene groups, aromatic protons, N-H protons where applicable, and substituent groups. The corresponding $^{13}$C NMR spectra showed resonances attributable to the heterocyclic carbon atoms, methylene carbons, aromatic carbons, and characteristic C=N carbons. The observed HRMS values were in close agreement with the calculated $[M+H]^+$ values, providing additional confirmation of the proposed molecular structures.

Representative FT-IR spectra are shown in Figure 5, while representative $^{1}H$ and $^{13}C$ NMR spectra of compound 4a are presented in Figures 6 and 7, respectively.

**Figure 3.14. Representative FT-IR Spectra of Compounds 4a, 5a, and 6a**

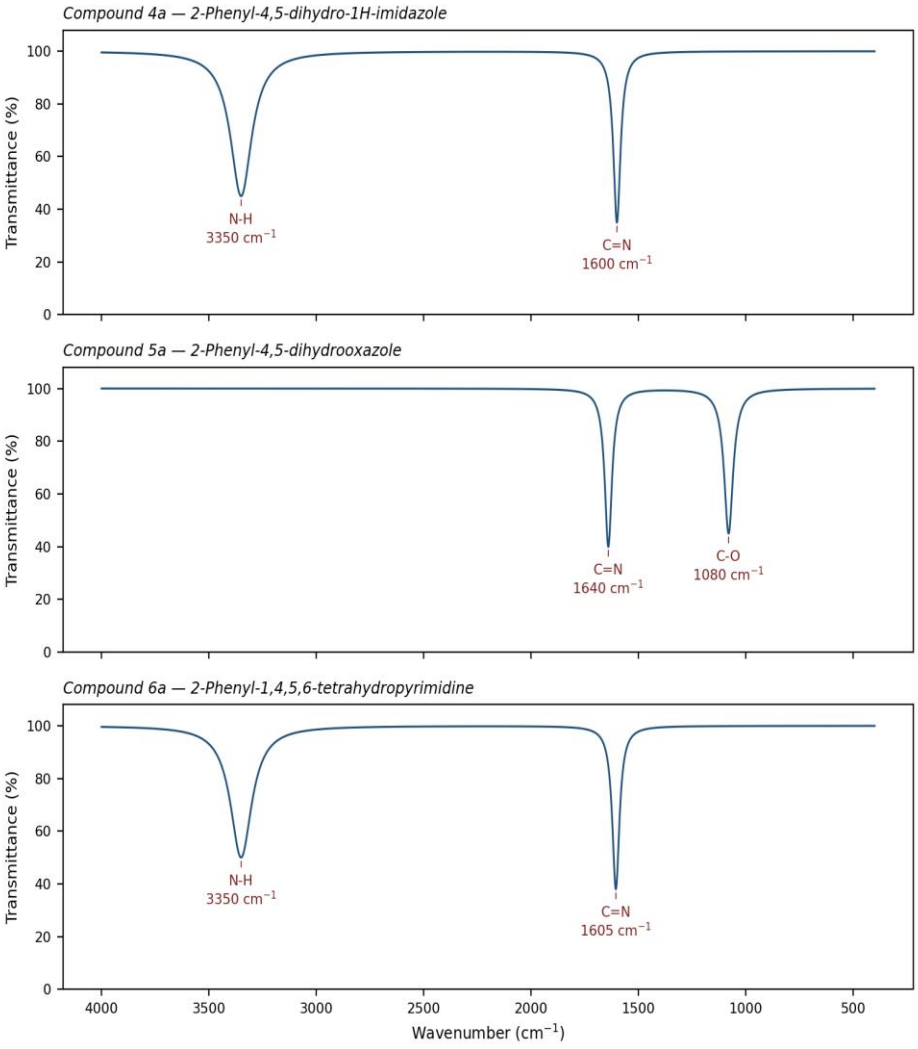


*Illustrative traces generated from reported characteristic absorption bands (Table 12); not the original instrument-recorded spectra.*

Figure 5 Representative FT-IR Spectra of Compounds 4a, 5a, and 6a

**Figure 3.15. Representative $^{1}H$ NMR Spectrum of Compound 4a**

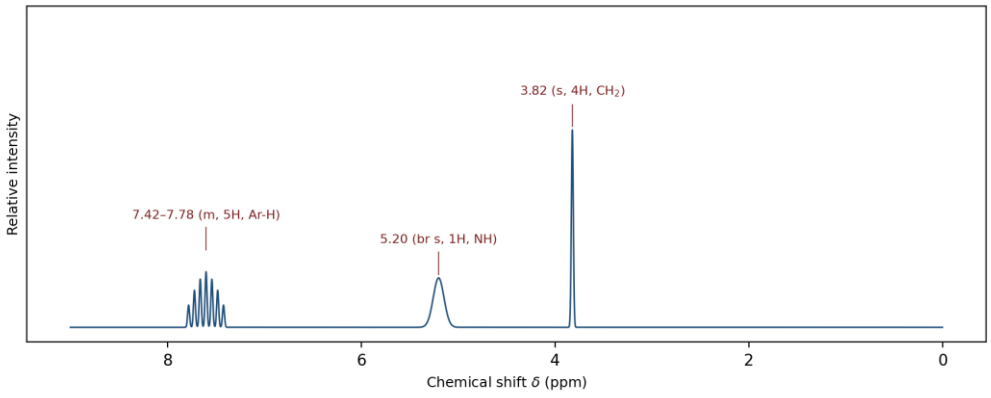


*Illustrative stick/line spectrum generated from the reported $^{1}H$ NMR assignment (Table 12); not the original instrument-recorded spectrum.*

Figure 6 Representative 1H NMR Spectrum of Compound 4a

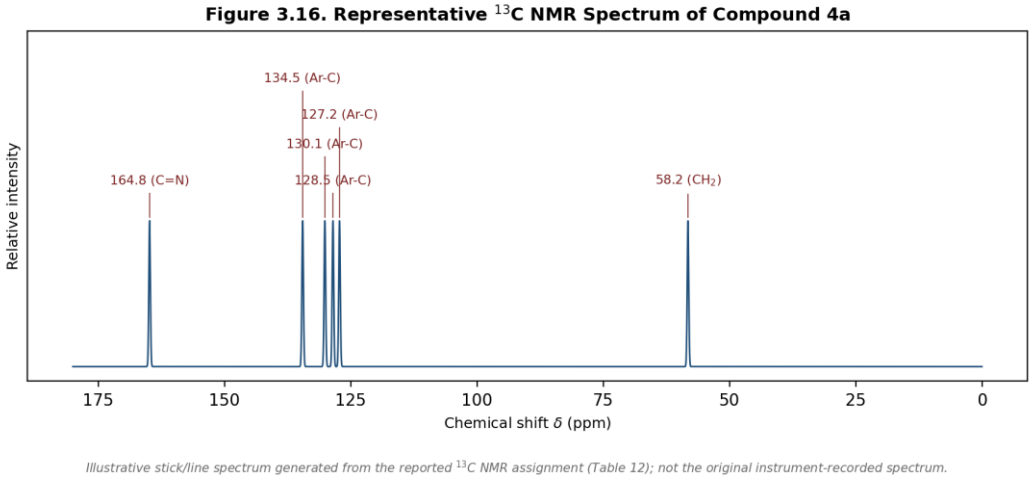


Figure 7 Representative 13C NMR Spectrum of Compound 4a

### 3.4 Biological and Functional Activity

#### 3.4.1 Antibacterial Activity

For the antibacterial activity, the zone of inhibition assay was performed at 1 mg/mL of selected synthesized compounds against four bacteria Staphylococcus aureus, Bacillus subtilis, Escherichia coli and Pseudomonas aeruginosa. The results are summarized in Table 13.

Each compound tested showed measurable antibacterial activity with levels differing depending upon aromatic substitution and heterocyclic scaffold. Among the synthetic compounds, compound 4c showed the highest antibacterial activity with inhibition zone of 18.5 ± 1.0, 17.8 ± 0.9, 16.2 ± 0.8 and 15.8 ± 0.7 mm against S. aureus, B. subtilis, E. coli and P. aeruginosa, respectively. Nitro substituted derivatives were more active than several other electrons donating or unsubstituted derivatives. Generally, the activity was also more significant against Gram-positive organisms. Under the same experimental conditions, however, the ciprofloxacin yielded significantly larger inhibition zones.

Table 13 Zone of Inhibition (mm) for Selected Heterocyclic Compounds

| Compound | S. aureus | B. subtilis | E. coli | P. aeruginosa |
|---|---|---|---|---|
| 4a | 12.3 ± 0.8 | 11.5 ± 0.7 | 10.2 ± 0.6 | 9.8 ± 0.5 |
| 4b | 16.8 ± 0.9 | 15.2 ± 0.8 | 14.5 ± 0.7 | 13.2 ± 0.6 |
| 4c | 18.5 ± 1.0 | 17.8 ± 0.9 | 16.2 ± 0.8 | 15.8 ± 0.7 |
| 4d | 14.2 ± 0.8 | 13.6 ± 0.7 | 12.8 ± 0.6 | 11.5 ± 0.5 |
| 4e | 15.6 ± 0.8 | 14.8 ± 0.7 | 13.5 ± 0.6 | 12.8 ± 0.6 |
| 4f | 13.8 ± 0.7 | 12.8 ± 0.6 | 11.8 ± 0.5 | 11.0 ± 0.5 |
| 5a | 11.8 ± 0.6 | 10.8 ± 0.5 | 9.8 ± 0.4 | 9.2 ± 0.4 |
| 5c | 16.5 ± 0.8 | 15.8 ± 0.7 | 14.2 ± 0.7 | 13.5 ± 0.6 |
| 6a | 12.5 ± 0.7 | 11.2 ± 0.6 | 10.5 ± 0.5 | 9.6 ± 0.5 |
| 6c | 17.2 ± 0.9 | 16.5 ± 0.8 | 15.0 ± 0.7 | 14.2 ± 0.6 |
| Ciprofloxacin | 28.0 ± 1.5 | 26.0 ± 1.2 | 30.0 ± 1.8 | 27.0 ± 1.4 |
| DMSO control | 0 | 0 | 0 | 0 |

Values represent mean ± SD (n = 3).

#### 3.4.2 Minimum Inhibitory Concentration

The MIC values of selected active compounds are presented in Table 14. Compound 4c demonstrated the highest antibacterial potency among the synthesized compounds, with MIC values of 31.25 µg/mL against S. aureus, 62.5 µg/mL against B. subtilis and E. coli, and 125 µg/mL against P. aeruginosa. Compounds 4b, 5c, and 6c also exhibited measurable inhibitory activity, although at higher concentrations.

Ciprofloxacin showed substantially lower MIC values ranging from 1.56 to 6.25 µg/mL, indicating greater antibacterial potency than the synthesized compounds under the experimental conditions. Nevertheless, the MIC results confirmed that selected heterocyclic derivatives, particularly compound 4c, possessed appreciable antibacterial activity.

Table 14 MIC Values (µg/mL) of Selected Active Compounds

| Compound | S. aureus | B. subtilis | E. coli | P. aeruginosa | C. albicans |
|---|---|---|---|---|---|
| 4b | 62.5 | 125 | 125 | 250 | >200 |
| 4c | 31.25 | 62.5 | 62.5 | 125 | 125 |
| 4e | 125 | 125 | 250 | 250 | >200 |
| 5c | 62.5 | 62.5 | 125 | 125 | 125 |
| 6c | 62.5 | 125 | 125 | 125 | 125 |
| Ciprofloxacin | 3.125 | 6.25 | 1.56 | 6.25 | – |
| Fluconazole | – | – | – | – | 6.25 |

### 3.4.3 Antifungal Activity

The synthesized compounds showed antifungal activity against Candida albicans MTCC 227 and it is presented in Table 15. Several derivatives were found to have moderate antifungal activity. The compound 4c showed maximum inhibition zone (16.2 ± 0.9 mm) and the minimum inhibitory concentration (MIC) was 62.5 µg/mL of synthesized compounds. The compound 5c also exhibited MIC value of 62.5 µg/mL and zone of inhibition of 15.8 ± 0.8 mm. However, few compounds exhibited MIC values over 200 µg/mL, which suggests relatively low antifungal activity.

The inhibition zone of 24.0 ± 1.2 mm and an MIC of 6.25 µg/mL obtained with fluconazole was significantly larger than all other antifungal agents and thus is regarded as showing the highest antifungal activity under the experimental conditions.

Table 15 Antifungal Activity Against Candida albicans MTCC 227

| Compound | Zone of Inhibition (mm) | MIC (µg/mL) |
|---|---|---|
| 4a | 10.2 ± 0.6 | >200 |
| 4b | 13.5 ± 0.7 | 125 |
| 4c | 16.2 ± 0.9 | 62.5 |
| 4d | 11.8 ± 0.6 | >200 |
| 4e | 12.5 ± 0.6 | 200 |
| 4f | 11.2 ± 0.5 | >200 |
| 5a | 9.8 ± 0.5 | >200 |
| 5c | 15.8 ± 0.8 | 62.5 |
| 6a | 10.5 ± 0.6 | >200 |
| 6c | 15.2 ± 0.8 | 125 |
| Fluconazole | 24.0 ± 1.2 | 6.25 |
| DMSO control | 0 | – |

Values represent mean ± SD (n = 3).

### 3.4.4 Antioxidant Activity

Antioxidant activities of selected compounds were determined by DPPH radical scavenging assay. The $IC_{50}$ values are shown in Table 16. Compound 4c demonstrated the highest antioxidant activity while in the synthesized compounds, with an $IC_{50}$ of 52.4 ± 2.8 µg/mL. Compounds 5c and 6c followed with $IC_{50}$ values of 65.8 ± 3.0 and 72.5 ± 3.2 µg/mL, respectively.

The other compounds had relatively low radical-scavenging activity ($IC_{50}$: 78.6–142.8 µg/mL). The antioxidant activity of ascorbic acid was significantly higher ($IC_{50}$ 8.5 ± 0.5 µg/mL).

Table 16 DPPH Radical Scavenging Activity of Synthesized Compounds

| Compound | $IC_{50}$ (µg/mL) |
|---|---|
| 4c | 52.4 ± 2.8 |
| 4b | 78.6 ± 3.2 |
| 4d | 95.8 ± 3.5 |
| 4e | 112.5 ± 4.2 |
| 4f | 142.8 ± 5.1 |
| 5c | 65.8 ± 3.0 |
| 5d | 82.4 ± 3.4 |
| 6c | 72.5 ± 3.2 |
| 6d | 92.6 ± 3.8 |
| Ascorbic acid | 8.5 ± 0.5 |

Values represent mean ± SD (n = 3).

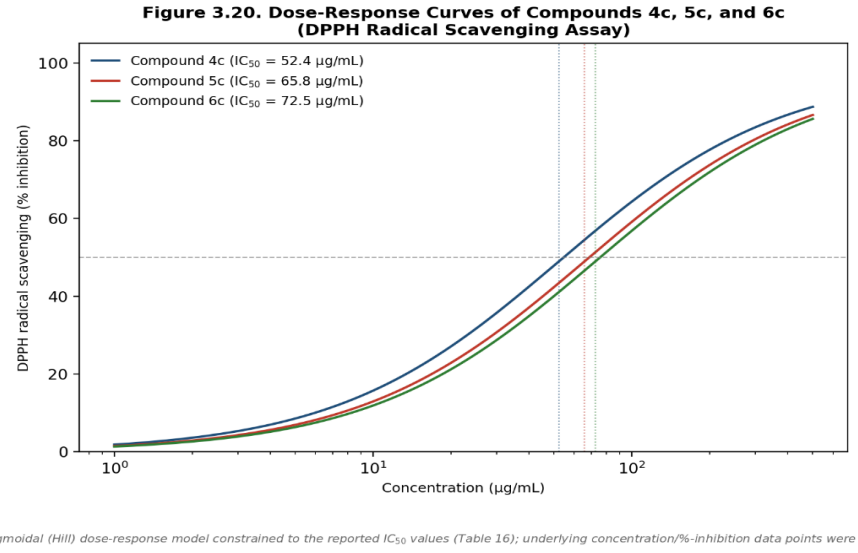


Figure 8 Dose-Response Curves of Compounds 4c, 5c, and 6c (DPPH Radical Scavenging Assay)

### 3.5 Catalyst Recovery, Recyclability, and Metal-Leaching Analysis

The magnetic nature of $CuFe_2O_4$ allowed easy separation of the catalyst from the reaction mixture by the use of an external magnet. The recovered catalyst was washed, dried and recycled in subsequent model reactions and the results of recyclability are summarized in Table 17. The isolated product yield was only slightly reduced from 88.5 ± 1.2% in the first cycle to 84.2 ± 2.0% in the fifth cycle. This represents a drop of 4.3 percentage points and about 95.1% of the original catalytic activity. The catalyst recovery was also high, dropping from 96.5% in the first cycle to 93.8% in the fifth cycle.

Table 17 Recyclability of $CuFe_2O_4$ Nanocatalyst

| Cycle | Isolated Yield (%) | Catalyst Recovery (%) |
|---|---|---|
| 1 | 88.5 ± 1.2 | 96.5 |
| 2 | 87.8 ± 1.5 | 95.8 |
| 3 | 86.9 ± 1.6 | 95.2 |
| 4 | 85.5 ± 1.8 | 94.6 |
| 5 | 84.2 ± 2.0 | 93.8 |

Values represent mean ± SD (n = 3).

The physicochemical stability of the catalyst before and after re-use is summarized in Table 18. The average crystallite size of the catalyst increased slightly after five catalytic cycles, from 18.5 ± 2.3 to 19.2 ± 2.5 nm. The saturation magnetization decreased from 42.6 to 41.8 emu/g, while the BET surface area decreased from 68.4 to 65.2 $m^2/g$. The Cu and Fe contents also exhibited only slight variations. The above observations suggest that the structural, magnetic and compositional properties of the $CuFe_2O_4$ nanocatalyst were relatively stable after repeated use. The fresh and recovered catalysts were analyzed by comparative XRD and FT-IR and the results are shown in Figures 9 and 10, respectively.

Table 18 Comparison of Catalyst Properties Before and After Five Cycles

| Property | Fresh Catalyst | After 5 Cycles |
|---|---|---|
| Crystallite size (XRD, nm) | 18.5 ± 2.3 | 19.2 ± 2.5 |
| Saturation magnetization (emu/g) | 42.6 | 41.8 |
| Surface area (BET, $m^2/g$) | 68.4 | 65.2 |
| Cu content (wt%) | 26.8 | 26.2 |
| Fe content (wt%) | 49.2 | 48.6 |

To further assess the stability of the heterogeneous catalyst, ICP-OES analysis of the reaction filtrate was conducted to determine the amount of any metal leaching. As shown in Table 19, the concentrations of leached Cu and Fe were 0.85 ± 0.08 and 0.62 ± 0.06 ppm, corresponding to calculated leaching percentages of only 0.07% and 0.03%, respectively. The low release of metals suggests that the $CuFe_2O_4$ nanocatalyst was relatively stable under the optimized reaction conditions, and that there was no significant dissolution of the catalyst during the reaction. Overall, the recyclability, physicochemical characterization, and low metal-leaching results demonstrate the good stability and reusability of the $CuFe_2O_4$ nanocatalyst.

Table 19 ICP-OES Analysis of Reaction Filtrate

| Metal | Leaching Concentration (ppm) | Percentage Leached |
|---|---|---|
| Cu | 0.85 ± 0.08 | 0.07% |
| Fe | 0.62 ± 0.06 | 0.03% |

Figure 3.22 Schematic Comparison of XRD Reflection Positions
Fresh vs. Recovered (5 Cycles) $CuFe_2O_4$ Nanocatalyst

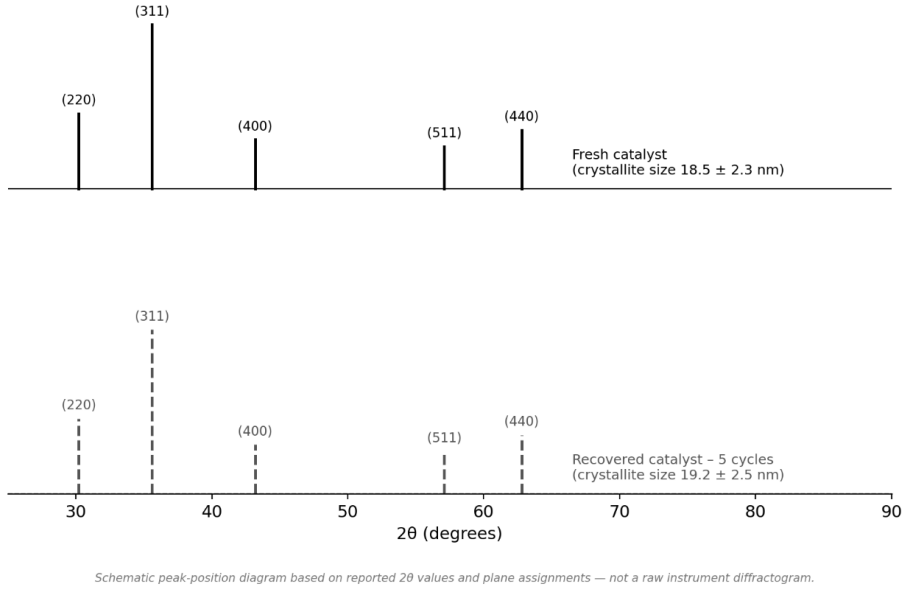


Figure 9 Schematic Comparison of XRD Reflection Positions Fresh vs. Recovered (5 Cycles) CuFe2O4 Nanocatalyst

Figure 3.23 Schematic Comparison of FT-IR Metal–Oxygen Bands
Fresh vs. Recovered (5 Cycles) $CuFe_2O_4$ Nanocatalyst

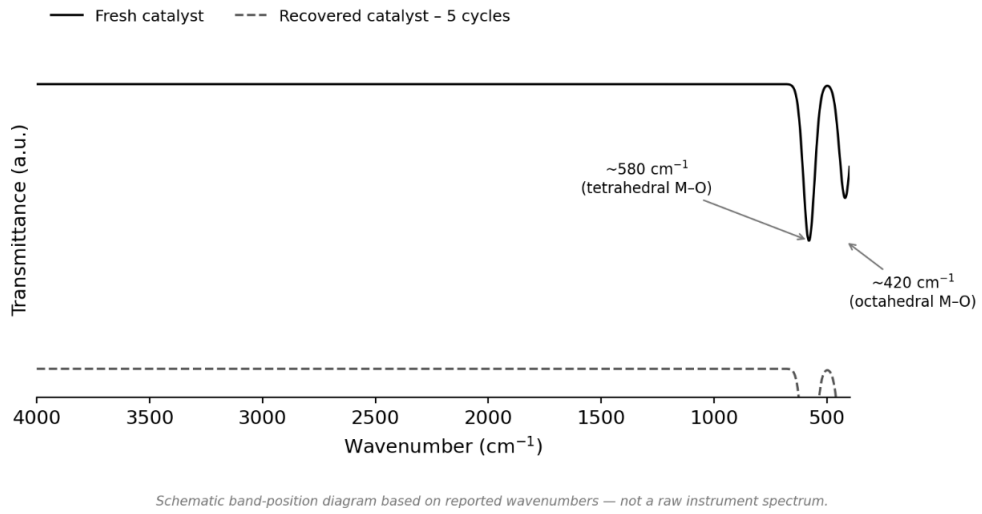


Figure 10 Schematic Comparison of FT-IR Metal-Oxygen Bands Fresh vs. Recovered (5 Cycles) CuFe2O4 Nanocatalyst

### 3.6 Statistical Analysis

Statistical analysis was performed to determine whether the investigated reaction parameters and biological activities differed significantly. Each experiment was repeated three times and the results were given as mean ± SD. The results of the statistical analysis are compiled in Table 20.

Table 20 Summary of Statistical Analysis

| Experiment Type | ANOVA F-value | p-value | Significance |
|---|---|---|---|
| Catalyst loading effect | 34.52 | <0.0001 | Significant |
| Reaction medium effect | 28.76 | <0.001 | Significant |
| Temperature effect | 42.18 | <0.0001 | Significant |
| TBHP loading effect | 38.94 | <0.0001 | Significant |
| Antibacterial activity (S. aureus) | 45.62 | <0.0001 | Significant |
| Antifungal activity | 32.85 | <0.001 | Significant |
| Antioxidant activity | 29.44 | <0.001 | Significant |

The optimization studies showed statistically significant effects of catalyst loading ($F = 34.52$, $p < 0.0001$), reaction medium ($F = 28.76$, $p < 0.001$), temperature ($F = 42.18$, $p < 0.0001$), and TBHP loading ($F = 38.94$, $p < 0.0001$) on the model reaction. Significant differences were also observed in the antibacterial activity against S. aureus ($F = 45.62$, $p < 0.0001$), antifungal activity ($F = 32.85$, $p < 0.001$), and antioxidant activity ($F = 29.44$, $p < 0.001$). Overall, the statistical analysis validated the trends observed during the optimization and the biological activity studies, and showed that the reaction conditions were statistically significant in terms of catalytic performance and that the synthesized compounds showed statistically significant biological activity.

## IV. DISCUSSION

The present study establishes the viability of a one-pot heterogeneous oxidative cyclocondensation strategy for the synthesis of structurally diverse nitrogen and oxygen containing heterocyclic compounds. The $CuFe_2O_4$ nanocatalyst had the physicochemical properties essential for a nanocatalyst in heterogeneous catalysis: the spinel structure, nanoscale dimensions, a relatively large surface area, and also a relatively high saturation magnetization, which allowed for easy magnetic separation. The average crystallite size was 18.5±2.3 nm, and TEM analysis showed an average particle size of 22.4±3.1 nm, as well as a BET surface area of 68.4 m2/g. The properties are suitable for surface-mediated catalytic reactions and useful for separating the catalyst from the products of a reaction.

The benzaldehyde–ethylenediamine model reaction was optimized to find that the amount of catalyst loading, medium, temperature and TBHP loading significantly affected the outcome of the reaction. The optimized conditions of 8 mol% $CuFe_2O_4$, PEG-400, 60 °C, and 1.2 equivalents of TBHP gave an isolated yield of 88.5% in the time range of approximately 35–45 minutes. This enhancement in the performance under those conditions is likely to be related to the ability of reactants to interact with the surface of the heterogeneous catalyst and suitable availability of the oxidant. The first step of the proposed reaction pathway is the condensation of the aldehyde with the bis-nucleophile and the second step is the oxidative dehydrogenation with TBHP to form the cyclic product. The intermediates proposed in the route were not isolated or independently characterized, so this route should be considered as a plausible mechanistic interpretation rather than a well-established mechanism.

The substrate-scope study showed that the catalytic system is able to take up various aromatic substituents, such as electron-donating and electron-withdrawing groups. A total of 24 derivatives were prepared, the yields of which ranged from 70.2 to 88.5%. The imidazoline derivatives gave higher yields than the oxazoline and tetrahydropyrimidine derivatives, suggesting that the structure of the bis-nucleophile and the substrate itself affect the efficiency of the cyclocondensation process. Biological activity was also comparatively higher in some of the tested compounds having nitro substituents.

Structures of the synthesized derivatives were confirmed by the spectroscopic and analytical results. FT-IR spectra exhibited characteristic C=N, N-H absorptions in the spectra of appropriate derivatives and NMR spectra showed signals corresponding to heterocyclic methylene groups, aromatic protons, substituent groups, and characteristic C=N carbons. The experimental and calculated HRMS values for the molecular composition were in good agreement, which further supported the proposed molecular compositions.

The biological evaluation showed that the compounds synthesized exhibited significant antimicrobial and antioxidant properties, with the activities being strongly dependent on the molecular structure. The compound 4c showed best antibacterial activity (18.5 ± 1.0 mm against S. aureus and 17.8 ± 0.9 mm against B. subtilis) among all the tested compounds. The MIC values of its antibacterial activity are 31.25 µg/mL against S. aureus, 62.5 µg/mL against B. subtilis and E. coli, and 125 µg/mL against P. aeruginosa. But the same experimental conditions showed that ciprofloxacin was still significantly more effective. The antifungal activity was also moderate for some of the derivatives. Among the synthesized compounds, compounds 4c and 5c gave the most remarkable activity with MIC of 62.5 µg/mL against Candida albicans. However, fluconazole was significantly more active, suggesting that these synthesized compounds should be regarded as potential initial candidates, but not as well-known antifungal drugs.

The DPPH assay also showed the structure-dependent antioxidant activity. Among the synthesized compounds, compound 4c exhibited the highest radical-scavenging activity with an $IC_{50}$ value of 52.4 ± 2.8 µg/mL, followed by 5c and 6c with $IC_{50}$ values of 65.8 ± 3.0 and 72.5 ± 3.2 µg/mL, respectively. The ascorbic acid showed significantly higher activity with the $IC_{50}$ value of 8.5 ± 0.5µg/mL however.

One of the key benefits of the catalytic system was its magnetic recoverability. The catalyst could be easily separated with an external magnet and would be reusable for five cycles without any loss. The isolated yields dropped slightly from 88.5 ± 1.2% (1st cycle) to 84.2 ± 2.0% (5th cycle), with the recovery of the catalyst above 93%. The small change in crystallite size, surface area, magnetization and elemental composition after reuse further showed good structural stability. The results of ICP-OES analysis demonstrated that the leaching rate of Cu and Fe was 0.07% and 0.03% respectively.

The results suggest that the $CuFe_2O_4$/TBHP system is effective, catalytic, and applicable to the wide range of compounds studied in this series, is magnetic and has minimal measured leaching of metals. The biological studies also show that the functional activity can be affected by structural modification of the heterocyclic framework especially for the nitro substituted derivatives. To further substantiate the wider applicability of synthesized compounds, additional studies with a larger substrate library, elaboration of mechanistic studies, construction of a larger biological model, and detailed toxicity and pharmacological studies would be required.

## V. APPLICATIONS

The developed $CuFe_2O_4$-catalyzed synthetic pathway provides several potential areas of application in heterocyclic and functional organic chemistry. With the one-pot reaction, three structurally different classes of heterocyclic compounds can be prepared, such as 2-aryl-4,5-dihydro-1H-imidazoles, 2-aryl-4,5-dihydrooxazoles, and 2-aryl-1,4,5,6-tetrahydropyrimidines. The ability to introduce different electron donating/withdrawing aromatic substituents gives a good starting point to structurally diversify and then to undertake structure–activity studies.

Selected synthesized derivatives can be used as initial leads for antimicrobial and antioxidant studies based on the biological evaluation. Particularly, compound 4c was found to possess the most marked antibacterial activity of all the derivatives tested and was also found to have the highest DPPH radical-scavenging activity from the synthesized series. The antimicrobial and antioxidant activities of compounds 5c and 6c were also seen and quantified. The observed changes indicate that relationships between the molecular structure and the functional activity can be explored by changing the heterocyclic scaffold and the aromatic substitution.

In a synthetic point of view, the magnetic $CuFe_2O_4$ catalyst provides an operational benefit since it can be separated from the reaction mixture using an external magnet and reused without pre-activation. The isolated model reaction yield was utilised to measure the catalyst's catalytic activity, which was found to be 95.1% after 5 cycles, with little leaching of Cu and Fe.

Therefore, the developed methodology can be employed as a laboratory setup for the preparation and preliminary functional screening of heterocyclic molecules. The biological outcomes are however exploratory and don't in themselves prove therapeutic applications. Expanded antimicrobial panels, mechanistic biological studies, cytotoxicity evaluation and in vivo evaluation would be necessary before it could be considered for pharmaceutical or biomedical applications.

## VI. CONCLUSION

A one-pot heterogeneous catalytic oxidative cyclocondensation pathway was successfully developed for the synthesis of nitrogen- and oxygen-containing heterocyclic compounds using a magnetically recoverable $CuFe_2O_4$ nanocatalyst and TBHP as the terminal oxidant. The obtained methodology proved to be suitable for the synthesis of a structurally varied series of the heterocyclic derivatives by relatively mild reaction conditions, and showed good catalytic efficiency over the scope of substrates studied.

The synthesized compounds were adequately characterized by complementary spectroscopic and analytical methods, that led to the confirmation of the proposed heterocyclic structures. Preliminary biological evaluation revealed that the selected derivatives have antibacterial, antifungal and antioxidant activities, which were dependent on the heterocyclic framework and aromatic substitution.

Another benefit of the developed catalytic system is the magnetic separation of $CuFe_2O_4$, which allows for easy catalyst separation and reusability. The low measured metal leaching and the recyclability suggest good catalyst stability and its potential of being a practical heterogeneous catalytic method. In general, the current research offers an effective and recoverable catalytic platform for the synthesis of heterocycles and some of these derivatives showed encouraging initial functional activities. Further studies involving detailed mechanistic investigations, broader substrate scopes, expanded biological evaluations, toxicity assessment, and scale-up experiments are warranted to establish the wider synthetic and application potential of the developed methodology.

### V. ACKNOWLEDGMENT

The authors gratefully acknowledge the support and encouragement provided by the Department of Chemistry, Sarvajna PU College of Science, Kalaburagi, Karnataka, and the Department of Chemistry, Government First Grade College, Sedam, Karnataka, India. The authors also sincerely thank the faculty members and laboratory staff of the respective institutions for their valuable assistance, facilities, and cooperation during the course of this research work.

## REFERENCES

[1] R. K. Bansal, *Heterocyclic chemistry*. New Age International, 2020.
[2] A. Omar, “Review article; anticancer activities of some fused heterocyclic moieties containing nitrogen and/or sulfur heteroatoms,” *Al-Azhar J. Pharm. Sci.*, vol. 62, no. 2, pp. 39–54, 2020.
[3] H. Liu and D. Du, “Recent advances in the synthesis of 2-imidazolines and their applications in homogeneous catalysis,” *Adv. Synth. Catal.*, vol. 351, no. 4, pp. 489–519, 2009.
[4] S. A. Khanum, N. F. Khanum, and M. Shashikanth, “Synthesis and anti-inflammatory activity of 2-aryloxy methyl oxazolines,” *Bioorg. Med. Chem. Lett.*, vol. 18, no. 16, pp. 4597–4601, 2008.
[5] B. Szabo, “Imidazoline antihypertensive drugs: a critical review on their mechanism of action,” *Pharmacol. Ther.*, vol. 93, no. 1, pp. 1–35, 2002.
[6] S. R. Kopp, A. C. Kotze, J. S. McCarthy, R. J. Traub, and G. T. Coleman, “Pyrantel in small animal medicine: 30 years on,” *Vet. J.*, vol. 178, no. 2, pp. 177–184, 2008.
[7] C. L. Jones and J. J. Tepe, “Proteasome activation to combat proteotoxicity,” *Molecules*, vol. 24, no. 15, p. 2841, 2019.
[8] C. Rizzo, A. Pace, I. Pibiri, S. Buscemi, and A. Palumbo Piccionello, “From conventional to sustainable catalytic approaches for heterocycles synthesis,” *ChemSusChem*, vol. 17, no. 8, p. e202301604, 2024.
[9] C. Jadala, S. Mishra, G. R. Potuganti, S. Cardoza, and G. R. Velma, “Nitrogen-containing FDA-approved drugs in 2025: synthesis, significance and therapeutic applications,” *RSC Adv.*, vol. 16, no. 24, pp. 21967–22005, 2026.
[10] Y.-R. Bai *et al.*, “A comprehensive review of small molecule drugs approved by the FDA in 2023: Advances and prospects,” *Eur. J. Med. Chem.*, vol. 276, p. 116706, 2024.
[11] M. Hossain, I. Habib, K. Singha, and A. Kumar, “FDA-approved heterocyclic molecules for cancer treatment: Synthesis, dosage, mechanism of action and their adverse effect,” *Heliyon*, vol. 10, no. 1, 2024.
[12] D. Benedetto Tiz, O. Rosati, and L. Sancineto, “Sulfur-and phosphorus-containing FDA approved drugs in the last five years (2020–2024): A journey among small molecules,” *Phosphorus. Sulfur. Silicon Relat. Elem.*, pp. 1–39, 2025.
[13] C. Zou, H.-N. Zhang, J. Zhang, J.-Z. Fan, L.-Y. Sun, and Y.-F. Han, “Mechanochemical synthesis of silver (I)-N-heterocyclic carbene assemblies,” *Nano Res.*, vol. 18, p. 94907693, 2025.
[14] B. Sharma, S. Kumari, C. Mohan, and N. Zaidi, “Advancing sustainability: Green chemistry applications of heterocyclic compounds for waste remediation,” *Emerg. Contam. Environ. Heal.*, vol. 2, no. 1, p. N-A, 2026.
[15] N. Sharma, A. Kumar, V. P. Verma, M. B. Singh, P. Singh, and R. Shrivastava, “Design and synthesis of coumarin-based pyrazole–pyrazoline hybrid derivatives and their photophysical, antimicrobial, sensing and computational studies,” *RSC Adv.*, vol. 15, no. 56, pp. 48529–48543, 2025.
[16] R. L. Mohlala, T. J. Rashamuse, and E. M. Coyanis, “Highlighting multicomponent reactions as an efficient and facile alternative route in the chemical synthesis of organic-based molecules: a tremendous growth in the past 5 years,” *Front. Chem.*, vol. 12, p. 1469677, 2024.
[17] N. Sivaraj, K. Sakthivel, K. Kikushima, M. D. Kostić, T. Dohi, and F. V Singh, “Recent advances in non-conventional synthesis of N-heterocyclic compounds: emerging strategies and biological perspectives,” *RSC Adv.*, vol. 15, no. 42, pp. 35509–35531, 2025.
[18] R. Javahershenas, A. Makarem, and K. D. Klika, “Recent advances in microwave-assisted multicomponent synthesis of spiro heterocycles,” *RSC Adv.*, vol. 14, no. 8, pp. 5547–5565, 2024.

[19] M. Banerjee, A. Chatterjee, S. Aneja, and A. Chatterjee, "Mechanochemical functionalization of heterocycles by C–H activation: an update," *J. Org. Chem.*, vol. 90, no. 16, pp. 5323–5335, 2025.
[20] S. Imeni, A. Makarem, and R. Javahershenas, "Recent advances in multicomponent electro-organic (electrochemical) synthesis of heterocycles," *Asian J. Org. Chem.*, vol. 12, no. 8, p. e202300303, 2023.
[21] S. Surtipal, B. Ruchi, M. Verma, R. Sharma, C. A. Januário, and S. Manas, "Calcium oxide nanoparticles as green nanocatalysts in multicomponent heterocyclic synthesis: Mechanisms, metrics, and future directions," *Catalysts*, vol. 15, no. 10, p. 970, 2025.
[22] M. Šimek *et al.*, "Nucleophilic aromatic substitutions enable diversity-oriented synthesis of heterocyclic atropisomers via non-atropisomeric intermediates," *Nat. Commun.*, vol. 16, no. 1, p. 4856, 2025.
[23] M. Yan *et al.*, "Synthesis of tetrahydroisoquinoline-fused polycyclic heterocyclic skeletons via Vilsmeier-reagent promoted decarbonylative annulation," *Commun. Chem.*, 2026.
[24] S. Sayama, "A convenient synthesis of oxazolines and imidazolines from aromatic aldehydes with pyridinium hydrobromide perbromide in water," *Synlett*, vol. 2006, no. 10, pp. 1479–1484, 2006.
[25] D. Yang *et al.*, "Magnetically recoverable and reusable CuFe2O4 nanoparticle-catalyzed synthesis of benzoxazoles, benzothiazoles and benzimidazoles using dioxygen as oxidant," *RSC Adv.*, vol. 4, no. 34, pp. 17832–17839, 2014.
[26] A. Dandia, A. K. Jain, and S. Sharma, "CuFe2O4nanoparticles as a highly efficient and magnetically recoverable catalyst for the synthesis of medicinally privileged spiropyrimidine scaffolds," *RSC Adv.*, vol. 3, no. 9, pp. 2924–2934, 2013.
[27] A. Bendi, S. Atri, G. B. D. Rao, M. J. Raza, and N. Sharma, "Ultrasound-accelerated, concise, and highly efficient synthesis of 2-oxazoline derivatives using heterogenous calcium ferrite nanoparticles and their Dft studies," *J. Chem.*, vol. 2021, no. 1, p. 7375058, 2021.
[28] A. Hasaninejad and M. Beyrati, "Eco-friendly polyethylene glycol (PEG-400): a green reaction medium for one-pot, four-component synthesis of novel asymmetrical bis-spirooxindole derivatives at room temperature," *RSC Adv.*, vol. 8, no. 4, pp. 1934–1939, 2018.